Highly efficient broadband sum-frequency generation in the visible wavelength range

Huseyin Cankaya,[1,2,*] Anne-Laure Calendron,[1,2] Haim Suchowski,[3] and Franz X. Kärtner[1,2,4]

[1]*Center for Free-Electron Laser Science, Deutsches Elektronen Synchrotron, and Department of Physics, University of Hamburg, Notkestrasse 85, 22607 Hamburg, Germany*

[2]*The Hamburg Centre for Ultrafast Imaging, Universität Hamburg, Luruper Chaussee 149, 22761 Hamburg, Germany*

[3]*NSF Nano-scale Science and Engineering (NSEC), University of California, Berkeley, California 94720, USA*

[4]*Department of Electrical Engineering and Computer Science and Research Laboratory of Electronics, Massachusetts Institute of Technology, Cambridge, Massachusetts 02139, USA*

**Corresponding author: hcankaya@gmail.com*

Received February 3, 2014; revised March 27, 2014; accepted April 4, 2014; posted April 7, 2014 (Doc. ID 205918); published May 8, 2014

We report on efficient broadband sum-frequency generation, converting a 140 THz near-infrared bandwidth to the visible regime with photon conversion efficiency greater than 90%. Using a 20-mm-long aperiodically adiabatively poled KTP crystal, the spectral range 660–990 nm was converted to 405–500 nm using a strong pump wave at 1030 nm. The photon conversion efficiency was confirmed to be $92 \pm 0.5\%$ when pumped with an intensity of 0.94 GW/cm^2. Our experimental results agreed very well with analytic predictions and numerical simulations. © 2014 Optical Society of America

OCIS codes: (320.7110) Ultrafast nonlinear optics; (320.7090) Ultrafast lasers; (190.4410) Nonlinear optics, parametric processes; (190.7110) Ultrafast nonlinear optics.

http://dx.doi.org/10.1364/OL.39.002912

Optical parametric amplifiers (OPAs) enable broadband amplification with relatively high efficiency. For these amplifier systems, seed sources with nanojoule (nJ) energy level are favorable to avoid excessive superfluorescence effects in the amplified pulse. Ti:sapphire oscillators are good candidates for seeding of OPAs because of the high multi-nJ output pulse energy, well-developed CEP stabilization techniques, and ultrabroadband spectral coverage in the near-infrared region. However, this coverage is limited to the near-infrared regime, thus restricting the seed bandwidth of the OPAs.

Three-wave mixing processes inside a nonlinear crystal enable wavelength conversion to wavelength regions that are not covered by other broadband laser systems. The conversion bandwidth of the nonlinear processes depends on the phase mismatch parameter among pump, signal, and idler pulses, where for ultrafast pulses, the signal bandwidth can reach more than 200 THz [1]. Such broad bandwidths are challenging to phase match. Thin nonlinear crystals can support the broadband three-wave mixing process but at the expense of efficiency. Several techniques have been suggested to enhance the efficiency over a broad bandwidth, such as quasi-phase-matching with chirped grating design [2,3], phase matching in bulk polycrystal [4], achromatic phase matching [5–8], temperature gradient phase matching in a quasi-phase-matched crystal [9], and use of several crystals [2]. While these methods improve efficiency or bandwidth of the conversion process, all exhibit a trade-off between bandwidth and efficiency. By using the adiabatic frequency conversion method, based on a mechanism analogous to rapid adiabatic passage from atomic physics, one can overcome this limit [10].

From the analogy, it follows that to produce an adiabatic passage of energy from a seed pulse to the frequency converted pulse, the phase mismatch parameter should vary slowly during the conversion process, from a large negative phase mismatch value to a large positive one (or vice versa). The phase mismatch Δk among the seed (ω_1), pump (ω_p), and sum-frequency generation (SFG) ($\omega_3 = \omega_1 + \omega_p$) beams must be swept from $\Delta k < 0$ to $\Delta k > 0$ along the propagation axis in a nonlinear crystal. In the presence of a sufficiently strong pump field, energy is efficiently converted from frequency ω_1 to ω_3. Thus, the adiabatic method relaxes the restriction of minimizing the phase mismatch among the interacting beams, and instead requires Δk to be varied slowly (i.e., adiabatically) during the nonlinear interaction, allowing the system to adapt to the changes caused by the slow phase mismatch. Mathematically, adiabatic evolution means that the system remains in one of its eigenmodes for the entire dynamical evolution.

The amount of adiabaticity is determined by the adiabaticity inequality and can be estimated by the Landau–Zener adiabaticity criteria, detailed in Refs. [10–13]. Using the adiabaticity criteria for all frequencies involved, a full transition from the signal (the lower state in two level atomic system) to the idler is possible (the excited state in a two-level atomic system), thus efficient conversion for a broadband source is achieved. The conversion of each frequency component occurs in a different location along the nonlinear crystal, correlating with the location of $\Delta k(z) \approx 0$ for the interacting waves involved. When the phase matching is tuned over the entire signal spectrum, one can obtain full-photon conversion for very broadband spectra [5–8].

In this Letter, we demonstrate adiabatic SFG (A-SFG) with over $92 \pm 0.5\%$ photon conversion efficiency using an aperiodically adiabatively poled KTP crystal [10–13]. In our demonstration, a pulse spectrum covering the range between 660 and 990 nm produced by white-light generation is converted by a slowly varying quasi-phase-matching grating in a 20-mm-long KTP crystal to the spectral range between 405 and 500 nm, corresponding

to a 140 THz bandwidth. To our knowledge, this is the highest efficiency and most broadband photon upconversion reported from a SFG process. Previous research reported only 11% photon conversion efficiency for an ultrashort pulse with 44 THz bandwidth centered around 765 nm [12], and conversion efficiency of 74% for a relatively narrowband tunable seed source between 1400 and 1700 nm [11]. The adiabatic conversion technique was applied not only for SFG but also difference-frequency generation [14,15] and OPAs to enhance the efficiency [16,17], reporting nearly full-photon conversion efficiency in the mid-infrared [14,15].

The schematic of the experimental setup is shown in Fig. 1. A Yb:KYW chirped pulse regenerative amplifier system (Amplitude S-Pulse HP2), delivering 1 mJ pulses at 1 kHz with pulse duration of 450 fs, centered at 1030 nm wavelength, was used to generate both the signal and pump pulses for A-SFG. A small portion of the pump pulse (~1.5%) was used for pumping the white-light supercontinuum stage, while only 2% of it was used to pump the A-SFG stage. The rest of the pump was kept for further experiments. The output of the amplifier was split by using thin-film polarizers (TFPs) coupled with half-wave plates ($\lambda/2s$). The white-light supercontinuum generated in a 6-mm-long YAG crystal was used as a signal source to test the crystal for A-SFG. The pump beam was focused inside the YAG crystal by using a lens (L1) with 100 mm focal length. The spotsize was measured to be 25 μm. The pump intensity was finely adjusted by employing a variable attenuator before L1. From the white-light process, we obtained a continuum covering from 510 nm to the mid-infrared region. The output of the white light was collimated by using an off-axis parabolic silver mirror.

An aperiodically poled KTP crystal (A-PKTP) for A-SFG was designed supporting a seed spectral range between 660 and 990 nm. The poling period of the KTP crystal was varied between 2.1 and 5.6 μm, allowing phase matching for the signal wavelength range from 660 to 990 nm. The corresponding period of the grating, with length of 20 mm, is given by the function $K_{\mathrm{QPM}} = -30z^3 - 120z^2 - 1900z - 11300$ [1/mm] in terms of distance along the propagation direction (z), centered at the middle of the crystal, where the design principles for the quasi-phase-matched grating follow those given in Refs. [10,11]. In contrast to the previous works, the polynomial dependency of the function was directly linked to bandwidth and to the dispersion of the materials, which allowed us to preserve the adiabaticity condition for the broadband design. By filtering out the spectral range with a combination of short- and long-pass filters (FS1), we have verified the functionality of the nonlinear crystal in this specific wavelength range.

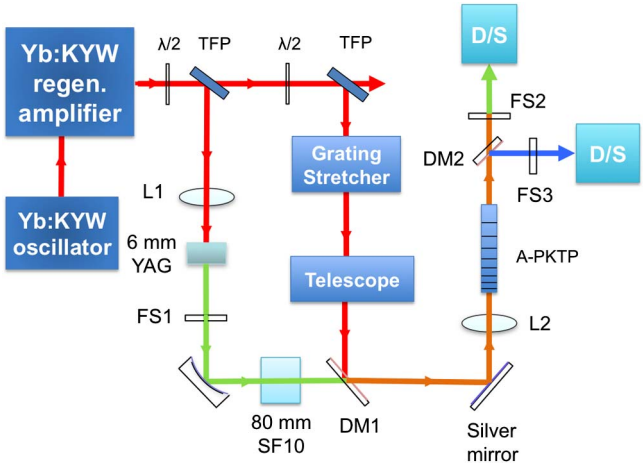

Fig. 1. Schematic of the adiabatic SFG setup. The signal to be covered was generated via white-light continuum inside a YAG crystal.

To avoid temporal walk-off between seed and pump pulses, both seed and the pump pulses were stretched. The pump pulse was stretched to 10 ps using a grating pair, where the gold-coated gratings with 1200 mm^{-1} grove density were oriented close to the blaze angle and separated by 12 cm from each other, while the seed pulse was stretched using an 80-mm-long slab of SF10. The glass thickness was determined by optimizing the photon conversion efficiency in the A-SFG process. The pulse duration of the white-light continuum at the entrance of the crystal was estimated to be 9.6 ps by taking into account dispersion of the YAG and SF10 plates.

The signal and pump pulses were combined by a dichroic mirror (DM1) which was highly reflective (99.9%) at 1030 nm and 95% transmissive for the signal range. The average power of the signal was measured to be 6.5 μW before the crystal, corresponding to 6.5 nJ per pulse. Both pump and signal pulses were then focused inside the A-PKTP by using a lens (L2) with 500 mm focal length. A telescope was employed in the pump arm to match the spotsize of the pump with the signal at the focus inside the KTP crystal. The radii at $1/e^2$ of the pump beam having a Gaussian beam profile were measured to be 53 and 57 μm the in x and y axes, while the radius of the signal was measured to be 55 μm. An aperture was used in the signal line before focusing to clear up the spatial shape of the beam and reduce the effect of spatial chirp in the outer part of the beam originated from generation of white-light continuum. During the experiments, the pump energy at the entrance of the crystal was varied up to 1.05 μJ. Assuming 15% Fresnel reflection loss from the surface of the crystal and an effective area of πw_0^2 (w_0 is the radius at $1/e^2$), this corresponds to an intensity of 0.94 $\mathrm{GW/cm}^2$ inside the crystal. To determine the conversion efficiency in the presence of the pump, the depletion of the signal was measured with both a photodetector (EOT, ET-4000) and an intensity calibrated spectrometer (Ocean Optics, HR4000) (D/S). From the measured signals with and without the presence of the pump, we have calculated the actual photon-number conversion efficiency. The SFG signal and the parasitic second-harmonic generation (SHG) signal at 515 nm due to the strong pump were separated by using a dichroic mirror (DM2), which was highly reflective (>99%) for the SFG range and transmissive (>90%) at signal and pump wavelengths. During the efficiency measurement, two bandpass filters (FS2) were employed to avoid the strong pump and the residual SHG signal present after DM2.

The spectrum of the white-light continuum before the crystal is shown in Fig. 2(a). To match the design signal wavelength range of the chirped KTP crystal, the

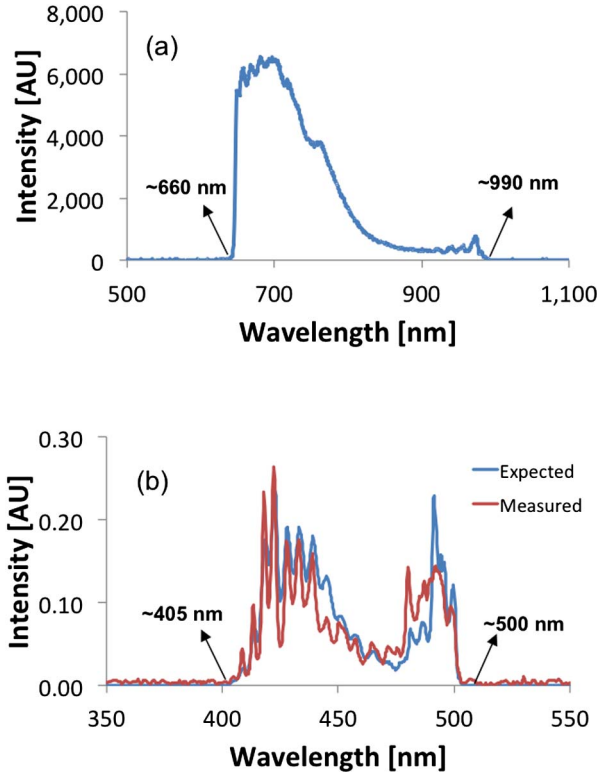

Fig. 2. (a) Spectrum of white-light super-continuum after the short- and long-pass filters (FS1). (b) Measured and expected spectrum for A-SFG selected by short-pass filters (FS3).

spectrum was filtered to cover the range between 660 and 990 nm. The ripples that are shown close to the lower and higher wavelength edges of the spectrum are due to the transmission of the filters (FS1). In Fig. 2(b), the measured and expected spectra of the SFG signal are shown. The same spectrometer was used for the acquisition of the SFG spectra. During the measurement of the SFG spectrum, the parasitic SHG signal was suppressed by using two low-pass filters (FS3). The expected SFG spectrum was calculated from the signal spectrum by taking into account the transmission through the short-pass filters. The ripples in the SFG spectrum are due to the transmission spectrum of the filters (FS3) used during the measurement. As can be seen from Fig. 2(b), there is an excellent agreement between the expected and measured SFG specta.

Figure 3(a) shows the spectra of the white-light supercontinuum after the filters (FS2) in the absence and presence of pump light with an intensity of 0.50 GW/cm^2. The modulations in the spectra were due to filters used to cut the pump and residual second harmonic resulting from the strong pumping. As can be seen, in the presence of the pump pulse, nearly uniform spectral depletion of the signal was observed. The discrepancy with the expected uniform spectral depletion was attributed to tolerances in the manufacturing of the aperiodically poled grating. Figure 3(b) shows the integrated photon conversion efficiency over the spectrum as a function of pump intensity. This curve exhibits an asymptotic behavior as a function of pump intensity, which is also consistent with the model described in Ref. [17]. When the pump intensity increased to

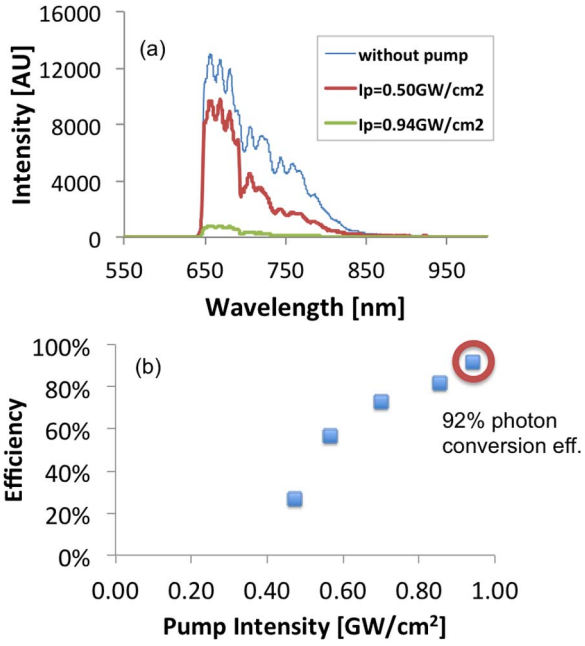

Fig. 3. (a) Signal spectra in the absence and presence of the pump pulse with intensity of 0.50 GW/cm^2 and 0.94 GW/cm^2. (b) Photon conversion efficiency in the A-SFG process as a function of pump intensity. The measurement accuracy was ±0.5%.

0.94 GW/cm^2, the SFG photon conversion efficiency increased up to 92 ± 0.5%. Above that intensity value, we observed repreducible damages on the surface of the crystal.

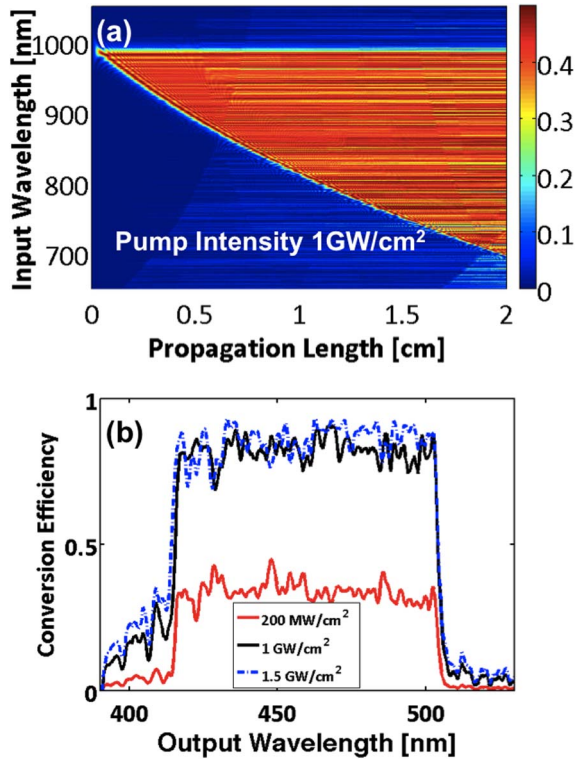

Fig. 4. (a) Simulation for photon conversion efficiency along the crystal as a function of signal wavelength for pump intensity level 1 GW/cm^2 and (b) simulated conversion efficiency at the end of the crystal as a function of wavelength for various pumping levels.

Figure 4(a) shows numerical simulations of the photon conversion efficiency along the aperiodically poled KTP as a function of signal wavelength for a pumping level of 1 GW/cm^2. The simulation, based on the finite difference method, was done for several pump intensities. As can be seen from the simulation, the conversion efficiency was constant along the crystal, which is also consistent with the experimentally measured signal depletion shown in Fig. 3(a). In Fig. 4(b), the conversion efficiency at the end of the crystal ($L = 2$ cm) is shown as a function of signal wavelength for three pumping levels: 200 MW/cm^2, 1 GW/cm^2, and 1.5 GW/cm^2. As can be seen, for a further increase in the pump intensity from 1 to 1.5 GW/cm^2, the conversion efficiency would increase only incrementally, following the prediction of the Landau–Zener adiabatic theory.

In conclusion, we experimentally demonstrated highly efficient SFG via Landau–Zener adiabatic transfer in an aperiodically poled KTP crystal (A-PKTP) for the spectral signal range of 660 to 990 nm. The photon conversion efficiency was measured to be $92 \pm 0.5\%$ for a very broad spectrum converted to 405–500 nm when the pump intensity was close to 1 GW/cm^2. This is the highest conversion efficiency demonstrated to date for SFG, to the best of our knowledge. Such broadband visible spectra can be used to seed a visible OPA for high harmonic generation or electron tip emission experiments.

This work has been supported by the excellence cluster "The Hamburg Centre for Ultrafast Imaging—Structure, Dynamics and Control of Matter at the Atomic Scale" of the Deutsche Forschungsgemeinschaft. The authors acknowledge many helpful discussions with G. Cirmi and O. D. Mücke about white-light continuum generation.

References

1. R. Ell, U. Morgner, F. X. Kärtner, J. G. Fujimoto, E. P. Ippen, V. Scheuer, G. Angelow, and T. Tschudi, Opt. Lett. **26**, 373 (2001).
2. M. Baudrier-Raybaut, R. Haidar, Ph. Kupecek, Ph. Lemasson, and E. Rosencher, Nature **432**, 374 (2004).
3. M. Arbore, A. Galvanauskas, D. Harter, M. Chou, and M. M. Fejer, Opt. Lett. **22**, 1341 (1997).
4. K. Mizuuchi, K. Yamamoto, M. Kato, and H. Sato, IEEE J. Quantum Electron. **30**, 1596 (1994).
5. O. E. Martinez, IEEE J. Quantum Electron. **25**, 2464 (1989).
6. G. Szab and Z. Bor, Appl. Phys. B **50**, 51 (1990).
7. T. R. Zhang, H. R. Choo, and M. C. Downer, Appl. Opt. **29**, 3927 (1990).
8. J. J. Huang, L. Y. Zhang, W. C. Zhang, S. R. Yan, S. Z. Pu, and W. X. Ren, J. Opt. Soc. Am. B **30**, 431 (2013).
9. Y. L. Lee, Y.-C. Noh, C. Jung, T. J. Yu, D.-K. Ko, and J. Lee, Opt. Express **11**, 2813 (2003).
10. H. Suchowski, D. Oron, A. Arie, and Y. Silberberg, Phys. Rev. A **78**, 063821 (2008).
11. H. Suchowski, V. Prabhudesai, D. Oron, A. Arie, and Y. Silberberg, Opt. Express **17**, 12731 (2009).
12. H. Suchowski, B. D. Bruner, A. Ganany-Padowicz, I. Juwiler, A. Arie, and Y. Silberberg, Appl. Phys. B **105**, 697 (2011).
13. H. Suchowski, G. Porat, and A. Arie, "Adiabatic processes in frequency conversion," Laser Photon. Rev., doi:10.1002/lpor.201300107.
14. J. Moses, H. Suchowski, and F. X. Kärtner, Opt. Lett. **37**, 1589 (2012).
15. H. Suchowski, P. R. Krogen, S. W. Huang, F. X. Kärtner, and J. Moses, in *Conference on Lasers and Electro-Optics*, OSA Technical Digest (online) (Optical Society of America, 2013), paper JM3K.5.
16. C. R. Phillips and M. M. Fejer, Opt. Lett. **35**, 3093 (2010).
17. C. R. Phillips, C. Langrock, D. Chang, Y. W. Lin, L. Gallmann, and M. M. Fejer, J. Opt. Soc. Am. B **30**, 1551 (2013).